Design and Analysis of Thermal Management for High-Power-Density Converters in Sealed Enclosures*

Michael T. Zhang[1], Milan M. Jovanović[2], and Fred C. Lee[1]

[1]Virginia Power Electronics Center, The Bradley Department of Electrical Engineering
Virginia Polytechnic Institute and State University, Blacksburg, VA 24061-0111

[2]Delta Power Electronics Lab., Inc., 1872 Pratt Drive, Suite 1400, Blacksburg, VA 24060

ABSTRACT: The size of external ac/dc adapters and battery chargers used in today's portable electronic equipment, such as notebook computers and portable printers, continues to decrease, while their rated output power slowly but steadily increases. As a result of the increased power density of the state-of-the-art adapter/chargers, the thermal management of the generated heat has become one the of most challenging design tasks. In fact, to optimize thermal performance, improve product reliability, and shorten design time, sophisticated thermal modeling is becoming an integral part of the design cycle. This paper discusses thermal-design considerations for high-power-density converters in sealed enclosures using Computation Fluid Dynamics (CFD) simulation approach. The thermal-design optimization guidelines obtained by simulations were verified on an experimental, high-power-density, 36-W, off-line ac/dc notebook adapter.

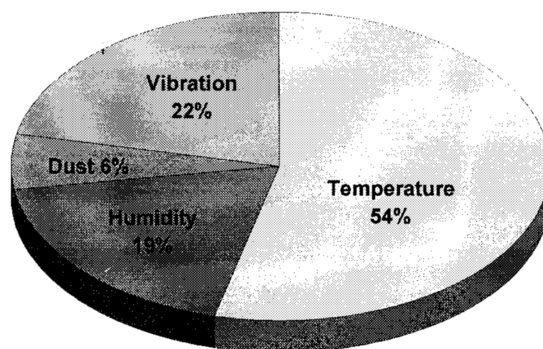

Fig. 1. Breakdown of premature failure causes of electronic equipment.

I. INTRODUCTION

As the power densities of power converters continue to grow, thermal issues are becoming extremely important and vital for the product quality. As illustrated in Fig. 1, which shows the primary causes of failures in electronic equipment, excessive temperatures of the critical components, such as semiconductors and transformers, are the dominant cause of equipment failures [1].

Power systems for portable and hand-held electronic equipment are usually housed in completely sealed enclosures due to safety reasons. Since the cooling of these systems primarily relies on natural convection, the effective management of the heat removal from a sealed enclosure poses a major thermal-design challenge. In fact, thermal design through thermal modeling and simulation is becoming an integral part of the design process because it is usually less time consuming and less expensive compared to the experimental cut-and-try approach.

In the past, thermal analysis has been mainly focused on component-level performance in the free-air environment or with estimated boundary conditions [2], [3]. Since components behave differently in a high-power-density environment due to thermal coupling with surrounding components, the accuracy and, therefore, the usefulness of the component-level thermal characterization are very limited in practical high-power-density systems. In addition, the extrapolation of the thermal-design performance from one converter structure to another is also of a limited value because of the possible lack of packaging similarities, different fluid velocities, and temperature gradients.

A more accurate approach to thermal analysis and modeling is the Computational Fluid Dynamics (CFD) approach which calculates heat transfer coefficients based on actual airflow conditions [4], [5]. As an example, the CFD-based Finite Volume Analysis (FVA) software Flotherm® [5], widely used in industry for modeling of electronic-equipment cooling, combines conduction, convection, and radiation effects and solves the entire coupled problem simultaneously. As a result, converter performance and component behavior can be simulated and analyzed in the actual operating environment.

In this paper, the general design aspects of the thermal management for high-power-density external adapter/chargers for portable electronic equipment are discussed. As an example, an off-line, 36-W flyback adapter is analyzed using CFD thermal modeling and simulation with Flotherm. The thermal modeling and simulation are performed for a number of packaging approaches. The simulation results are verified experimentally. Finally, the design guidelines for optimum thermal performance are outlined.

* This work was supported by Delta Electronic Ind. Co., Ltd., Taiwan.

0-7803-3704-2/97 $10.00 ©1997 IEEE

II. Estimation of Power Density Limits

Generally, in the adapters/chargers for portable electronic equipment housed in sealed enclosures, the heat generated by internally dissipated power is removed by natural convection and radiation from the enclosure surfaces. To comply with various agency requirements and internal specifications defined by portable-equipment manufacturers, the maximum surface temperature of the enclosure which is accessible to the user is limited. The most commonly encountered specification of the maximum-surface-temperature-limit is T_{surf} = 75 °C at ambient temperature T_{amb} = 40 °C, i.e., the maximum allowable surface-temperature rise above the ambient temperature is ΔT_{surf}^{max} = 35 °C. To stay below the surface-temperature limit, the maximum allowable power dissipation within the enclosure, $P_{d(max)}$, must also be limited. Moreover, since the adapter/chargers are placed on another object (e.g. desk, floor, etc.), $P_{d(max)}$ is further restricted because the bottom surface of the enclosure almost does not participate in the heat transfer, except for a limited amount of conduction to the object it is placed on.

Besides the maximum-surface-temperature compliance, the internal, maximum temperatures of magnetic (transformer, EMI and output-filter inductors) and semiconductor (transistors, rectifiers, ICs) components must be kept below certain limits imposed by safety regulations and/or reliability concerns. Generally, for a given maximum surface temperature, allowable $P_{d(max)}$ is maximized if power dissipation is uniform within the volume of the enclosure. In other words, for a given enclosure, the maximum output power and, therefore, maximum power density, can be achieved if the power dissipation is uniform. In practical circuits, the power distribution is not uniform but is is distributed among the major power-stage components, such as the power transformer, rectifier(s), and switch(es). As a result, practical allowable $P_{d(max)}$ is somewhat smaller than that calculated for the ideal case, which assumes the uniform power distribution. Nevertheless, the knowledge of the ideal-case $P_{d(max)}$ is a useful piece of information which can be used to determine the upper limit of the power density for a given enclosure volume, conversion efficiency, and surface-temperature limit.

To quantify the maximum permissible uniform power dissipation for a given enclosure, the heat produced by $P_{d(max)}$ can be separated, based on the heat-transfer mechanism, into convective heat $P_{d(max)}^{cov}$ and radiative heat $P_{d(max)}^{rad}$. The convection heat transfer coefficients of a rectangular enclosure are given by [7]

$$h_c = \begin{cases} 2.3 \cdot 10^{-3}\left(\dfrac{\Delta T}{D}\right)^{0.25}, & \text{vertical surfaces, } D = h; \\ 1.8 \cdot 10^{-3}\left(\dfrac{\Delta T}{D}\right)^{0.25}, & \text{horizontal surfaces, } D = \dfrac{2lw}{l+w}, \end{cases} \quad (1)$$

where $\Delta T = T_{surf} - T_{amb}$ is the surface temperature rise in °K (or °C), while l, w, and h are the length, the width and the height of the enclosure in inches, respectively. As can be seen from Eq. (1), the side-surfaces (vertical surfaces) have higher transfer coefficients than the top surface (horizontal surface). In addition, the side-surfaces heat transfer coefficient increases as height h decreases. Thus, for low-profile geometry, the side-surfaces are more effective in removing heat than the top surface. Assuming that the heat-transfer through the bottom surface is negligible and that the surface temperature distribution is uniform, the convective heat transfer is given by:

$$P_{d(max)}^{cov} = 10^{-3}\left[4.6(l+w)h^{0.75} + 1.8(lw)^{0.75}(l+w)^{0.25}\right]\Delta t^{1.25} \,. \quad (2)$$

Similarly, surface radiative heat transfer can be calculated using Boltzman's law as [7]

$$P_{d(max)}^{rad} = 3.66 \cdot 10^{-11} feA(T_{surf}^4 - T_{amb}^4)\,, \quad (3)$$

where f is the view factor, e is the emissivity, and A is the surface area in square inches. Due to the blockage effect of the desk, f is reduced to 0.5 for all side surfaces, and the bottom surface is practically ineffective. Therefore, using typical emmissivity value of e = 0.9 for plastic materials (materials of choice for adapters/chargers), Eq. (3) can be rewritten as

$$P_{d(max)}^{rad} = 3.3 \cdot 10^{-11}\left[(l+w)h + lw\right](T_{surf}^4 - T_{amb}^4)\,. \quad (4)$$

Combining Eqs. (2) and (4), the total permissible power dissipation for a given enclosure volume $V = l \cdot w \cdot h$ is determined by

$$\begin{aligned} P_{d(max)} &= P_{d(max)}^{cov} + P_{d(max)}^{rad} \\ &= 10^{-3}\left[4.6\frac{l+w}{(lw)^{0.75}}V^{0.75} + 1.8(lw)^{0.75}(l+w)^{0.25}\right]\Delta T^{1.25} \\ &\quad + 3.3 \cdot 10^{-11}\left[\frac{l+w}{lw}V + lw\right](T_{surf}^4 - T_{amb}^4)\,. \end{aligned} \quad (5)$$

Figure 2 shows the plot of the total permissible power dissipation $P_{d(max)}$ of an enclosure with volume V = 10 in^3 as a function of the aspect ratio w/l and h/l as a parameter, and with the constraint $l \geq w \geq h \geq 1$ in. From Fig. 2, it can be seen that $P_{d(max)}$ increases as the aspect ratio h/l decreases due to the increased heat transfer coefficient of the side surfaces. Also, for fixed h/l ratio, $P_{d(max)}$ is the largest when the aspect ratio w/l is the smallest, i.e., when side-surface area $A_{side} = 2(l+w)h$ is the maximum. In fact, due to the constraint $l \geq w \geq h \geq 1$ in, the minimum w/l is obtained for $w = h$, i.e., for the enclosure with the width equal to the height, as can be seen from Fig. 2. The length of such an enclosure is given by $l = V/(w \cdot h) = V/h^2$ [in]. Therefore, the maximum power-density can be obtained with a low-profile, rectangular-shape enclosure with square cross-sectional area ($w = h$). For

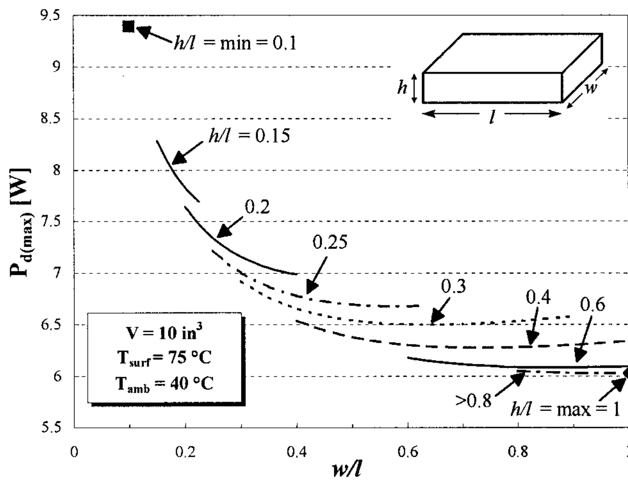

Fig. 2 Permissible power dissipation for enclosure of given volume ($V = 10$ in^3) as a function of the aspect ratio w/l and h/l as a parameter.

TABLE I

Comparison of analytically and numerically calculated permissible power dissipation for an enclosure with volume of $V = 10$ in^3.

Dimensions [in]	Analytical	Numerical	Error
$l = 10$, $w = 1$, $h = 1$	9.4 W	9.2 W	2.2%
$l = 3.2$, $w = 3.2$, $h = 1$	6.6	6.5	1.5%
$l = 2.2$, $w = 2.2$, $h = 2.2$	6.0 W	5.8 W	3.4%

example, for the 10 in^3 enclosure with the dimensions 10 in × 1 in × 1 in ($h/l = w/l = 0.1$), the maximum permissible power dissipation is $P_{d(max)} = 9.4$ W. On the other hand, for the same-volume enclosure with the square-footprint, i.e., 3.2 in × 3.2 in × 1 in, the maximum permissible power dissipation is only $P_{d(max)} = 6.6$ W.

The accuracy of the analytical calculations of $P_{d(max)}$ for the ideal-case of the uniform power dissipation is verified using Flotherm 3-D FDA simulator. Table I compares the analytical and numerical results for a number of different shapes of an enclosure with $V = 10$ in^3. As can be seen, the theoretical results are in a very good agreement with the numerically calculated results. The discrepancies are within 3.5%.

Knowing the maximum permissible power dissipation $P_{d(max)}$ and the conversion efficiency η, the maximum allowable output power, $P_{o(max)}$, for an enclosure with a given volume can be determined by

$$P_{o(max)} = P_{d(max)} \cdot \frac{\eta}{1-\eta}. \quad (6)$$

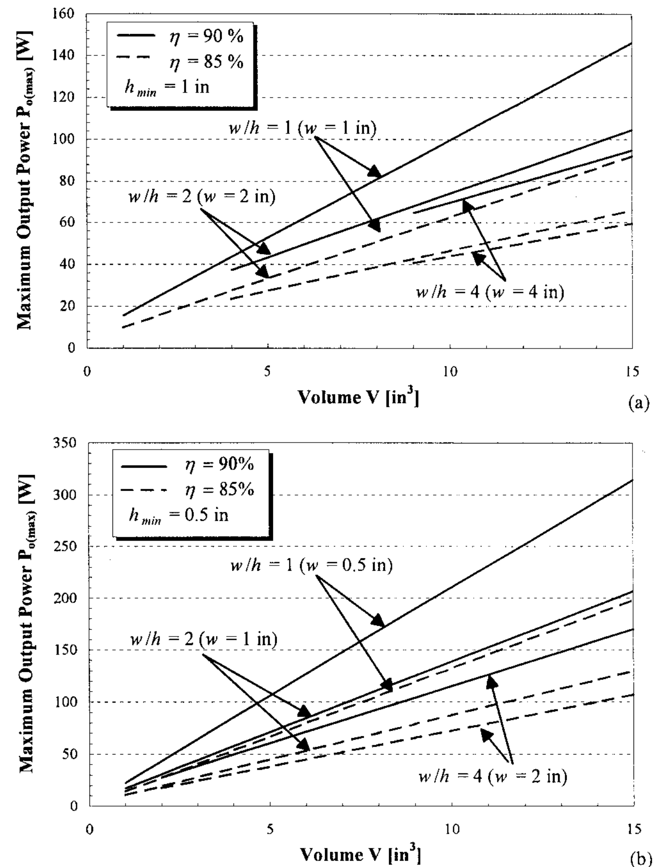

Fig. 3. Maximum achievable power as a function of enclosure volume and its cross-sectional aspect ratio w/h: (a) for $h_{min} = 1$ in; (b) for $h_{min} = 0.5$ in. Plots obtained by assuming uniform power distribution, $\Delta T_{surf} = 35$ °C, and conversion efficiency $\eta = 90\%$ (solid curves) and $\eta = 85\%$ (dashed curves)

Figure 3 shows $P_{o(max)}$ as a function of the enclosure volume and the enclosure cross-sectional aspect ratio w/h as a parameter, assuming 90% conversion efficiency (solid lines) and 85% conversion efficiency (dashed lines). Figure 3(a) was generated for the minimum profile of $h_{min} = 1$ in, while the minimum profile of $h_{min} = 0.5$ in was used in Fig. 3(b). As can be seen from Figs. 3(a) and 3(b), for any volume, the maximum output power is obtained for the square cross-sectional area ($w/h = 1$). In addition, more power can be delivered to the output for higher conversion efficiencies. Also, a lower profile enclosure has a higher maximum output power limit compared to the same-volume enclosure with a higher profile (higher h). Finally, it should be noted that constant slopes of the lines in Fig. 3 indicate that the power density, i.e., the ratio of the output power and the volume, is constant for given conversion efficiency and cross-sectional aspect ratio w/h. Based on the power dissipation consideration above, the maximum power density of 20 W/in^3 can be achieved for the enclosure with $h = 0.5$ in housing a 90% efficient converter.

III. INTERNAL TEMPERATURE DISTRIBUTION ANALYSIS

While the uniform-power-distribution approach is very useful for estimating the maximum theoretical allowable power dissipation in an enclosure, the practical maximum power dissipation is determined by the allowable temperature rises on the key components. In fact, in a practical circuit, the power dissipation and, therefore, the heat generation are non-uniform, since different amounts of power are generated on different components. As a result, the temperature distribution within the enclosure as well as on its surfaces is non-uniform. Since the maximum temperature rise of the electronics components is limited due to safety and/or reliability reasons, the practical maximum allowable power dissipation in an enclosure is determined by the temperature-rise limit of the critical components, i.e., by the maximum local (component) power dissipation. As a result, the maximum, practical allowable power dissipation is always smaller than the one estimated assuming the ideal uniform power distribution. Generally, the difference between the ideal estimate and the actual allowable power dissipation limit is dependent on the internal component placement (mechanical design) and packaging technique used.

To perform a 3-D temperature distribution analysis using Flotherm CFD software, the circuit layout and the power dissipation of the key components must be known. In this paper, a 36-W, off-line notebook adapter, packaged in a 3.8 in × 2.4 in × 1 in plastic enclosure without any vent holes is used to demonstrate the effectiveness of the CFD software in the thermal-design optimization. Figure 4 shows the mechanical structure of the adapter and the placement of its key components. The wooden board in Fig. 4 emulates a writing desk. The adapter uses a single-stage flyback topology to achieve 4 W/in^3 power density [8]. Figure 5 shows the measured efficiency and the total internal power loss at full load as a function of the line voltage [8]. As can be seen from Fig. 5, from the thermal-analysis point of view, the worst operating point is at low line (90 Vac), where the power loss is the maximum at 6.1 W due to high conduction losses. Figure 6 shows the calculated breakdown of the adapter losses at 90 Vac. As can be seen, the semiconductor component and the transformer account for the majority of the losses.

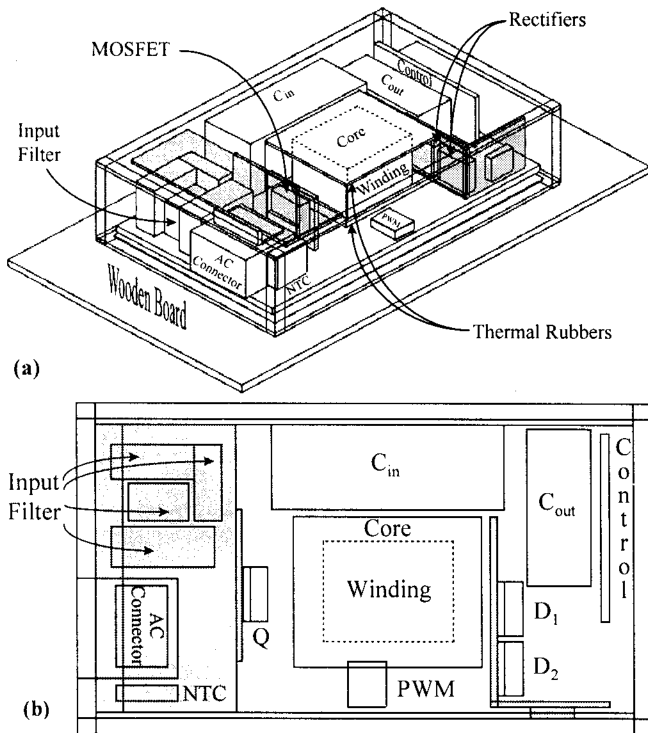

Fig. 4. Mechanical design and placement of key components in packaging design ❶: (a) 3-D view; (b) top view; (shaded areas are heatsinks.)

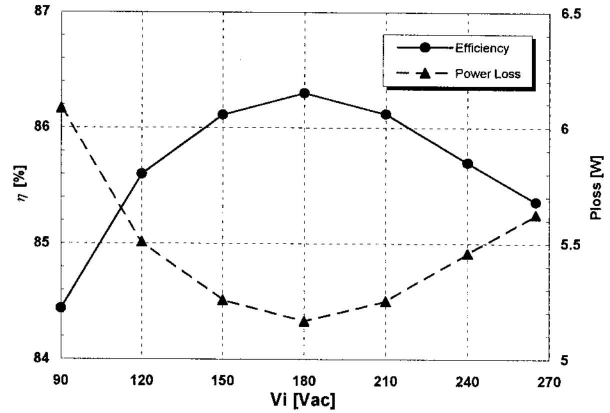

Fig. 5. Efficiency and total power loss of flyback adapter. Note that about 0.55-W loss is dissipated in the connecting cable and not included in the breakdown calculation.

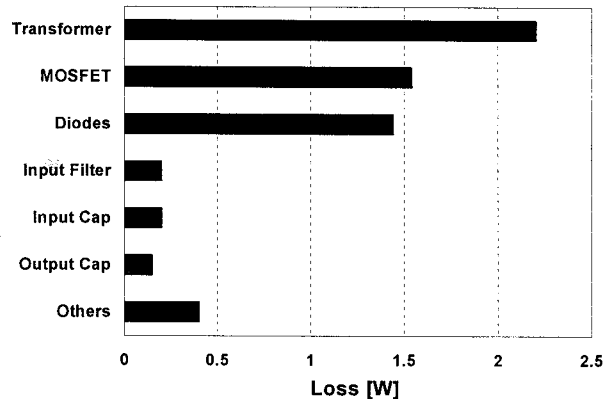

Fig. 6. Calculated adapter power-loss breakdown at 90 Vac.

IV. THERMAL MANAGEMENT OPTIMIZATION

Generally, in completely sealed enclosures the internal air flow velocity u is usually negligible (smaller than 0.01 m/s) [9]. In addition, within the enclosure, the densely

packaged components block the air flow. As a result, the internal heat convection is practically negligible so that the internal heat removal relies mainly on conduction.

It is very well-known that the internal thermal-conduction paths of heat generating sources should be designed so that they have low thermal resistance to the enclosure surfaces for minimum temperature gradients. According to Fig. 6, the major heat source in the adapter is the high-frequency transformer. Usually, the transformer is also the tallest component in an adapter. Therefore, to provide the most efficient heat-removal path, it is essential that the transformer be put in direct contact with the enclosure walls. However, for the transformer cores with center posts which have the winding axis parallel to the PCB surface as, for example, E, EPC, EFD and LP cores, only limited transformer surface area can be brought in contact with the enclosure due to the winding curvature. As a result, the thermal resistance between the transformer and the enclosure is increased. To remedy the problem, soft, thermally conductive materials (thermal rubbers) can be employed to fill the air gaps.

In this adapter, thermal rubbers are used to bring the top and bottom surfaces of the transformer in contact with the corresponding enclosure walls, as shown in Fig. 4. The effectiveness of the upward and downward heat-removal paths of the transformer is evaluated by different thermal rubber arrangements. Figure 7 shows the maximum temperatures of the transformer winding and the core obtained by Flotherm simulations for four rubber configurations: ① with both top and bottom 2-mm rubbers; ② without the bottom rubber; ③ with a 1-mm thick top rubber; ④ without any rubber. As can be seen from Fig. 7, the removal of the bottom rubber increases the transformer temperatures by only 2 °C. Therefore, the downward path is not essential for the transformer. However, decreasing the thickness of the top rubber by 50% results in a temperature rise of 4 °C for the winding and 10 °C for the core. Therefore, the top surface is the dominant heat-removal path for the transformer. Finally, from Fig. 7, it can be seen that configurations ① and ② are below the winding-isolation, class-B temperature limit of 110 °C, while configurations ③ and ④ exceed the limit.

The heat from the semiconductor devices is transferred to the enclosure surface by the heatsinks, which provide very effective heat removal paths due to their high metallic conductivity. As can be seen from Fig. 4, the inverted L-shape heatsink of MOSFET Q is in direct contact with the inside top surface of the enclosure, while the heatsink of rectifiers D_1 and D_2 is in contact with a side surface. To reduce the junction temperature of the primary-side MOSFET, which has the second largest power dissipation in the adapter, its junction-to-heatsink thermal resistance must be minimized. Since the junction-to-heatsink thermal resistance depends on the MOSFET case, a performance study utilizing Flotherm

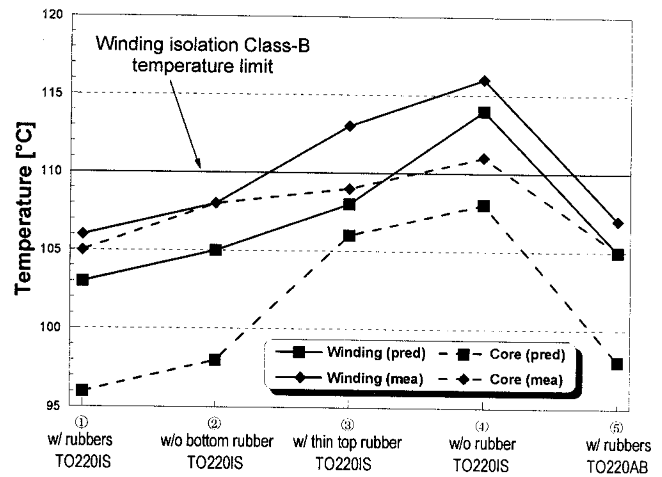

Fig. 7. Simulation (■) and experimental (◆) results of transformer temperatures with different rubber arrangements and different MOSFET case styles. Configurations ①-④ use MOSFET in TO220IS package (w/o tab), while configurations ⑤ uses TO220AB package (w/ tab)

simulation was conducted to compare and quantify the thermal performances of the MOSFETs in TO220AB and TO220IS case styles shown in Fig. 8. Since TO220AB has a metal mounting tab, which removes the heat more effectively from the small size silicon die because the mounting tab spreads the heat out laterally first and then vertically conducts the heat to the heatsink [10], it is expected that the TO220AB package should have better thermal performance compared to that of the TO220IS package. This conclusion was confirmed by simulations shown in Fig. 9 where the data for arrangement ⑤ were obtained for the circuit with a MOSFET in the TO220AB package and the top and bottom thermal rubbers. As can be seen from the comparison of arrangements ① and ⑤ in Fig. 9, the TO220AB package reduces the MOSFET temperature by 7 °C compared with the TO220IS package which does not have a mounting tab. At the same time, the transformer core and winding temperatures are also reduced due to a cooler MOSFET, as can be seen from Fig. 7. Therefore, as long as it does not conflict with the enclosure-profile specification, using a MOSFET in TO220AB package is a cost-effective solution which improves the thermal performance of the circuit.

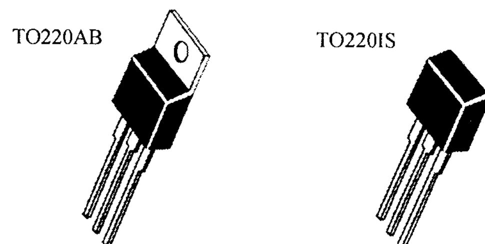

Fig. 8. Two package styles used to evaluate thermal behavior of primary MOSFET.

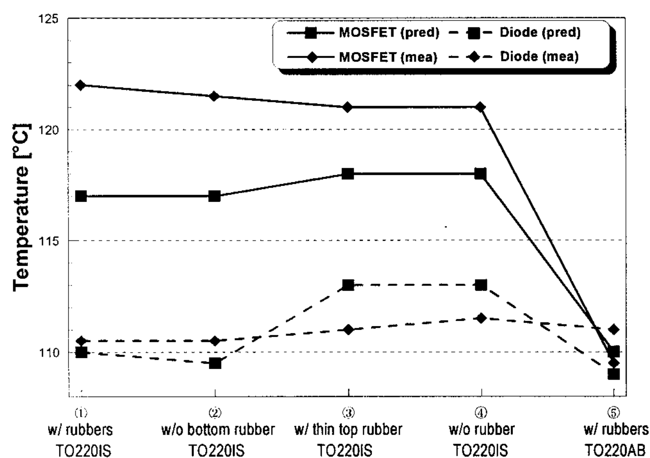

Fig. 9. Simulation (■) and experimental (◆) results of semiconductor junction temperatures with different thermal rubber arrangements and different MOSFET case styles.

The amount of heat that can be removed from enclosure surfaces is greatly influenced by the temperature rise and surface area. It is desirable to have a uniform surface temperature for convection and radiation. Therefore, hot spot elimination not only reduces single component failure, but also increases the cooling capability of the enclosure. Other than by a proper layout of the heat sources (which is restricted by the circuit topology as, for example, primary-to-secondary side isolation), the effective surface area can be maximized by using surface heat-spreaders which can distribute the heat laterally and achieve a more uniform temperature distribution. Surface heat-spreaders can be implemented either by wrapping a copper foil around the circuit and providing a contact between the foil and the enclosure, or by plating the spreader on the inner surface of the enclosure. Figure 10 shows the top-surface temperature maps of the enclosure adapter without and with a heat-spreader at the ambient temperature of T_{amb} = 40 °C. Without the heat-spreader (Fig. 10(a)), the transformer has the maximum surface temperature of 94 °C. With the heat-spreader (Fig. 10(b)), no hot-spot area is present, and the maximum surface temperature, which is still located above the transformer, is reduced to 79 °C. Simulations also show that the thickness of the heat-spreader is not critical, as long as its thermal conductivity is high, i.e., > 50 W/m°C. Since for high-frequency, switching-mode power supplies, radiated EMI shielding is usually required, the EMI shield can be used as a surface heat-spreader to reduce the cost.

However, even with the heat-spreader mounted on top of the transformer with the EPC core (packaging design denoted ❶), the maximum surface temperature of 79 °C, which occurs above the transformer, is still over the maximum allowable temperature of 75 °C. Therefore, to bring the top surface below 75 °C, the heat transfer from the transformer to the ambient needs to be improved. The necessary improvement in

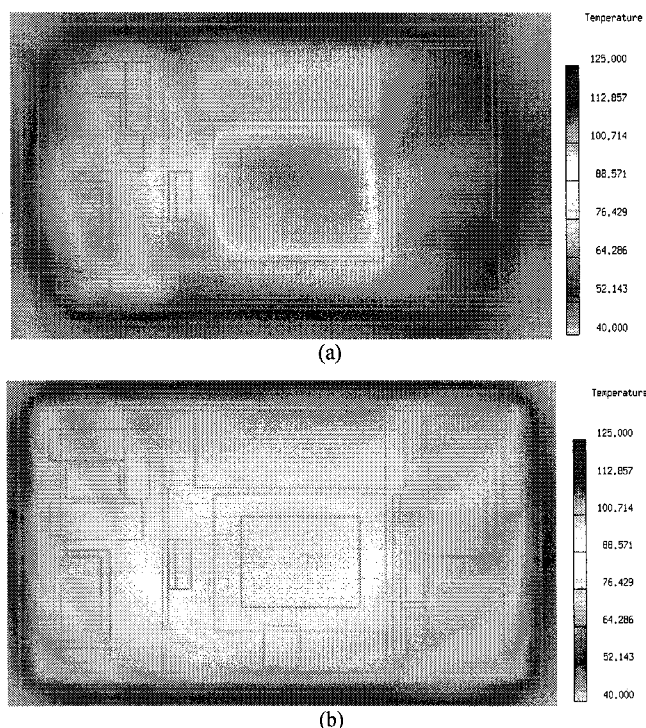

Fig. 10. Temperature maps of top surface of adapter: (a) w/o surface heat spreader; (b) with surface heat spreader.

the heat transfer can be achieved by using transformer core shapes with flat top surfaces such as pot or RM type cores, instead of EPC-type cores. As shown in Fig. 11(b), the horizontally wound windings in an RM core are not in the thermal conduction path. Therefore, the core can be put in a direct contact with the enclosure surfaces, i.e., without using thermal rubbers, for a more efficient heat removal. Generally, this configuration is more thermally effective for transformers where the core loss dominates over the winding loss.

With an RM or similar-type core, a more uniform surface temperature distribution can be obtained by replacing the separate transistor and rectifier heatsinks in packaging design ❶, shown in Fig. 4 with an integral heatsink (metal plate) in contact with the top, inner surface of the enclosure. This packaging approach denoted as packaging design ❷ is

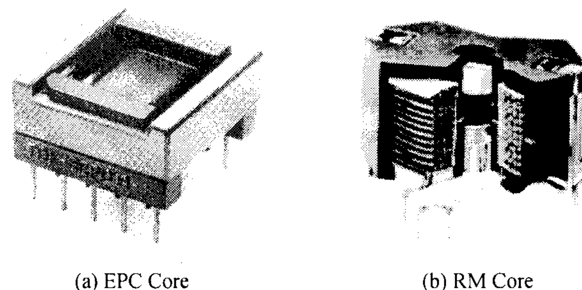

(a) EPC Core (b) RM Core

Fig. 11. Transformer core shapes: (a) EPC; (b) RM.

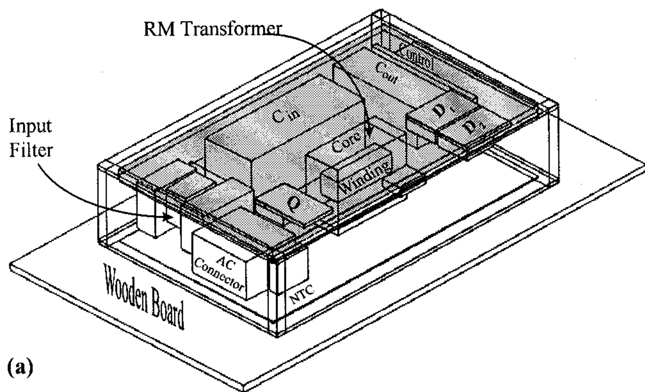

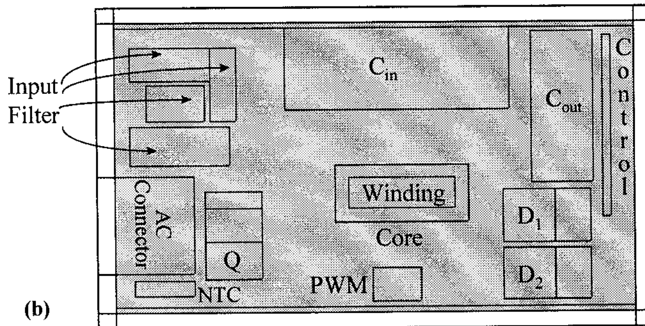

Fig. 12 Mechanical design and placement of key components in packaging design ❷: (a) 3-D view; (b) top view; (shaded area ▒ is heatsink.)

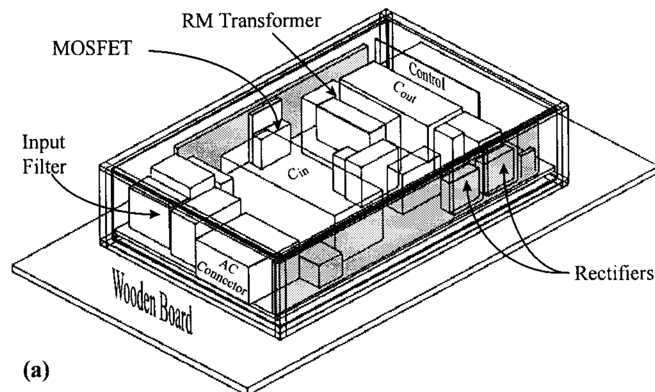

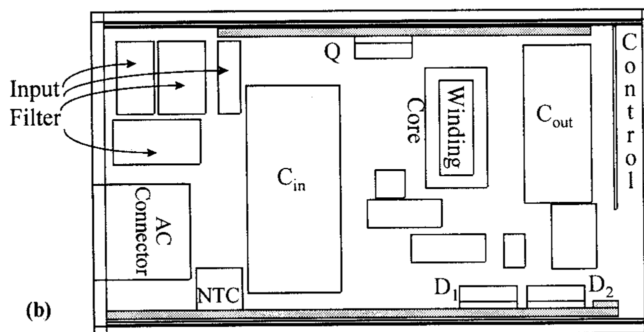

Fig. 13 Mechanical design and placement of key components in packaging design ❸: (a) 3-D view; (b) top view; (shaded areas ▒ are heatsinks.)

shown in Fig. 12. In packaging design ❷, the transistor and rectifiers are mounted flat on the heatsink. Since they are closer to the top surface of the enclosure, the heat conduction path is reduced, which results in better thermal performance.

However, in design ❷, the heat transfer of all the major heat sources (the semiconductors and the transformer) relies predominantly on the heat removal through top surface. As it was explained in Sec. II, the side surfaces of an enclosure are even more effective in heat removal than the top surface. To efficiently employ the side surfaces in the heat removal process, the packaging design ❸, shown in Fig. 13, can be used. In this design, the semiconductor devices are placed along the sides of the PCB and brought in contact with the side surfaces of the enclosure by two separate heatsinks. As a result, in this packaging approach, the heat removal from the transformer and the semiconductor devices is done through different surfaces. Namely, the heat from the transformer is removed through the top surface, while the removal of the heat from the transistor and rectifiers is done through different side surfaces.

The thermal behaviors of designs ❶-❸, shown in Figs. 4, 12, and 13, are evaluated by Flotherm simulations assuming ambient temperature of 40 °C. The results are summarized in Fig. 14. As can be seen from Fig. 14, design ❷ reduces the temperatures of the transistor and rectifiers by 12 °C and 11 °C, respectively, compared to those in design ❶. At the same time, the use of the RM transformer decreases the core temperature by 13 °C. Also, the winding temperature in design ❷ is 5 °C lower than that in design ❶, although the winding in the RM core is not in a direct contact with the heatsink.

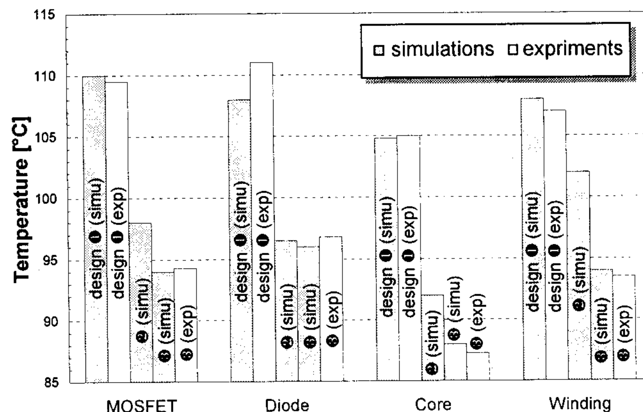

Fig. 14. Comparisons of temperatures of critical components for three packaging designs for Tamb = 40 °C. No experimental circuit for design ❷ was built.

By placing the semiconductor components close to the side surfaces, i.e., by virtually decoupling heat-removal paths of the transformer and semiconductors, design ❸ further improves the thermal performance. In design ❸, the MOSFET

temperature is 4 °C lower than that in design ❷. However, the temperature difference of the rectifier between designs ❷ and ❸ is insignificant (< 1 °C) because in design ❷ the rectifiers are close to the enclosure side surfaces (Fig. 12). Design ❸ also exhibits the lowest core and winding temperatures. In fact, the core temperature in design ❸ is 5 °C lower compared to that in design ❷, while the winding temperature in design ❸ is 8 °C lower than the corresponding temperature in design ❷. Finally, with the help of the EMI shield, which acts as a heat-spreader, the top surface temperature is uniformly distributed with a maximum value of 73 °C, as shown in Fig. 15. Therefore, for this application, design ❸ is the most cost-effective packaging approach with satisfying thermal performance.

It should also be noted that, according to Eq. (5), the maximum allowable power dissipation in the adapter-size enclosure (3.8 in × 2.4 in × 1 in), assuming a uniform power dissipation and the maximum surface temperature of 75 °C, is 6.3 W. In the adapter under consideration, the actual power loss was 6.1 W, while the surface temperature for design ❸ was slightly below the 75 °C limit. This less-than 5% difference between the ideal-case calculated and the actual allowable power dissipation implies that design ❸ distributes the dissipated heat almost uniformly throughout the enclosure.

Generally, thermal modeling is a fast and convenient tool for performance comparison studies. However, the accuracy of the thermal simulations is very much dependent on the accuracy of the model parameters, particularly those related to heat sources and thermal properties of materials. To evaluate the accuracy of the thermal modeling and simulations, Figs. 7, 9 and 14 also show the measured temperatures of the transformer and the semiconductor components of the 36-W adapter. In Figs. 7 and 9, the predicted temperatures are represented by ◆, while the measurement data are represented by ■. As can be seen from Figs. 7, 9, and 14, the predicted temperatures are within 10% of the measured temperatures. The main sources of the discrepancies are due to the following facts: (a) the physical properties of the material used are not fully known without taking material-property measurements; (b) for simplicity, some components are lumped together, e.g., the PCB and its traces are treated as one object with equivalent thermal properties; and (c) geometry is restricted to only rectangular shapes by the software [11]. However, more important than the absolute temperature predictions are the trends of the relative temperature changes for different thermal management designs because they point to the directions of thermal performance improvements. From Figs. 7, 9, and 14, it can be observed that thermal modeling gives very good trend predictions. Therefore, CFD thermal modeling has been found to be a fast and cost-effective tool for improving and optimizing the thermal management for high-density power converters.

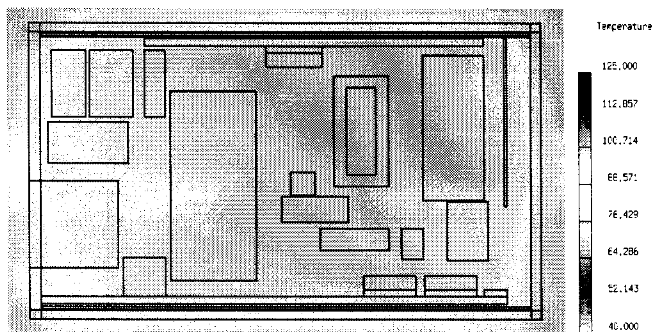

Fig. 15. Temperature map of top surface in packaging design ❸.

V. SUMMARY

The major design challenges in today's state-of-the-art, high-power-density, power-conversion circuits are increasingly related to the thermal management issues. In this paper, it has been demonstrated that the thermal-design optimization of a converter in a sealed enclosure can be performed on a cost-effective and time-efficient base by employing a thermal-analysis software based on the Computational-Fluid-Dynamics (CFD) approach. Using a 36-W, ac/dc, notebook adapter as an example, the results of the thermal-design optimizations obtained by CFD-based simulations were experimentally verified.

ACKNOWLEDGMENT

The authors wish to thank Mr. Albert Chang, manager of Adapter Group at Delta Electronics Inc., Taiwan for providing adapter samples, and Dr. Laszlo Huber of Delta Power Electronics Lab, Inc., for providing a part of the experimental results reported in this paper.

References

[1] C. Soule, "Yesterday's cooling won't work on tomorrow's electronics," *PCIM Magazine*, Nov., 1994, pp. 34-36.

[2] R. Parales Jr., "Solving the thermal design concerns of a low-voltage power supply using CFD modeling," *Proceedings of Flotherm Users' Conference*, May 1993.

[3] R. Ridley, M. Reynell, and S. Kern, "Thermal considerations for distributed Power converter systems," *Proceedings of IEEE Applied Power Electronics Conference*, Mar. 1993, pp. 866-872.

[4] T. Lee and M. Mahalingam, "Application of a CFD tool for system-level thermal simulation," *IEEE Trans. on Comp. Pack. & Manu. Tech.* - Part A. Vol. 17, No. 4, Dec. 1994, pp. 564-571.

[5] G. Crowe, "Thermal analysis and optimization of a small, high density dc power system by finite element analysis (FEA)," *Proc. IEEE Int. Telecommun. Energy Conf.*, Oct. 1996, pp. 718-722.

[6] *Flotherm® Instruction Manual*, Flomerics Limited, Surrey, England, 1995.

[7] A.D. Walker and D. Williams, "Thermal design considerations in the design and application of dc-dc converters," *Proceedings of IEEE Applied Power Electronics Conference*, Mar. 1996, pp. 990-996.

[8] L. Huber and M.M. Jovanović, "Evaluation of Flyback Topologies for Notebook AC/DC Adapter/Charger Applications," *Proceedings of High Frequency Power Conversion Conf.*, May 1995, pp. 284-294.

[9] T. Lee, B. Chambers, and M. Mahalingam, "Application of CFD technology to electronic thermal management," *Proceedings of 44th Electronic Components & Technology Conference*, May 1994, pp. 411-420.

[10] D.S. Steinberg, *Cooling techniques for electronic equipment*, New York: John Wiley & Sons, 1980.

[11] C. Lasance, "About the validation of CFD analysis of electronic system," *Proceedings of Flotherm Users Conference*, Sept. 1994.